Effect of network structure on phase transitions in queuing networks

Norbert Barankai, Attila Fekete, and Gábor Vattay
Department of the Physics of Complex Systems, Eötvös University, Pázmány Péter Sétány 1/A, H-1117 Budapest, Hungary
(Received 13 September 2012; published 13 December 2012)

Recently, De Martino *et al.* [J. Stat. Mech. (**2009**) P08023; Phys. Rev. E **79**, 015101 (2009)] have presented a general framework for the study of transportation phenomena on random networks with annealed disorder. One of their most significant achievements was a deeper understanding of the phase transition from the uncongested to the congested phase at a critical traffic load on uncorrelated networks. In this paper, we also study phase transition in transportation networks using a discrete time random walk model. Our aim is to establish a direct connection between the structure of an uncorrelated random graph with quenched disorder and the value of the critical traffic load. We show that if the network is dense, the quenched and annealed formulas for the critical loading probability coincide. For sparse graphs, higher-order corrections, related to the local structure of the network, appear.

DOI: 10.1103/PhysRevE.86.066111 PACS number(s): 89.75.Fb, 89.20.Ff, 68.35.Rh, 02.50.Ga

I. INTRODUCTION

During the past few decades, the physics community has witnessed enormous progress in the research on complex networks [1,2]. Transport processes on networks represent an important class of dynamical systems with a wide range of applications, including data traffic on the Internet, vehicle traffic on highways, virus spread between hosts, or rumor spread in social networks, to name but a few. A simple, general model can be used to describe these dynamical systems quite accurately, in which particles are transported between the nodes of a network.

In certain transport networks the particles are served by queues, residing at the nodes of the network. One of the most prominent examples is the Internet, where the data packets play the role of the particles. Queuing networks exhibit several interesting phenomena; for example, below a critical traffic intensity, the system is in a free state and the average queue length fluctuates around a finite value. Above a critical traffic load, however, one or more queues become congested and the average queue length diverges.

Various models have been developed to model Internet traffic. Deterministic and probabilistic routing strategies were compared in Ref. [3]. The authors of Ref. [4] studied a shortest-path routing model where the probability of packet transmission depended on the queue lengths. The authors of Ref. [5] studied how traffic congestion is affected by the capacity of the nodes in a simple shortest-path routing model. A more elaborate routing strategy was studied in Ref. [6], where the packets were forwarded to the neighbor that minimized an effective distance to the packet's destination. Beyond that, several attempts have been made to find routing strategies that are less sensitive to congestion [7–9].

Packet-level simulations of these models clearly indicate phase transitions between the free and congested phases, and several characteristics of the queuing networks exhibit power-law dependence from the traffic intensity close to the transition point [3–6,10]. The analytic description of these models, however, is rather limited, because even the simplest routing mechanism, namely the shortest-path routing, introduces nonlocal transport dynamics to the system.

In recent years, extensive research has been undertaken to discover the relationship between the topological properties of networks and the behavior of the dynamical processes on them [11–13]. A fundamental question is, if a dynamical system shows phase transition phenomena, how does the structure of the network affect the phase transition? In models with nonlocal transport dynamics, however, the analytic description of the phase transition has only been established for a few special networks, for example, lattices [3,14] or Cayley trees [4,5,10].

In recent papers by De Martino *et al.* [15,16], the authors studied the congestion phenomena on uncorrelated annealed networks. The authors introduced a traffic-aware congestion-control mechanism in their model and modeled the transport process with a simple random-walk process, instead of a nonlocal routing mechanism. It has been shown that the model exhibits both first- and second-order phase transition, depending on the parameters of a congestion control mechanism.

The main focus of our paper is to gain a deeper understanding of the relationship between the structural properties of the underlying graph and the congestion phenomena, that is the dynamics, and to give a generic description of the phase transition point in an arbitrary network with quenched disorder. Our model is similar to the one presented by De Martino *et al.* [15,16]. We approximate the particle-transport process with a discrete-time random-walk process, where packets are generated, absorbed, and move randomly in the network. Moreover, we assume that the delivery of the particles is locally homogeneous, that is the probability that a particle will be delivered from any node to its neighbor is uniform [15].

Our work differs from Refs. [15,16] in three important aspects, however. First, we do not consider any traffic-control mechanism in our study. Second, instead of using time-evolution equations, we apply an exact mean-field distribution in the long time limit and use spectral graph theory [17] to connect the structure of the network with the traffic dynamics. Third, instead of using networks with annealed disorder, our calculations are performed on an arbitrary graph but the consequences of our formulas are validated numerically only on uncorrelated random graphs with quenched disorder.

The paper is organized as follows. After presenting our model in detail in Sec. II, we derive relationships that connect

the critical traffic loading with the parameters of the model (Sec. III). In Secs. IV and V, we discuss the theoretical findings, and we then compare them to particle-level numerical simulations and numerical computations. Finally, we conclude our work in Sec. VI. Some of the details of the analytic calculation are presented in the Appendix.

II. THE MODEL

We model the transportation network by a simple connected graph with N nodes and M edges. Moreover, the dynamics of the transport networks are modeled by a discrete time stochastic process. The rules of the stochastic process are the following (see Fig. 1). At each node of the graph, there is a queue with infinite buffer capacity. In each time step, the first particle of each nonempty queue leaves the queue. A particle at node i will be either absorbed (i.e., leaves the queuing network) with probability μ_i, or it is delivered to another queue at node j, adjacent to node i, with probability P_{ji}.

The probability that a particle will be absorbed at node i can be expressed by $\mu_i = 1 - \sum_j P_{ji}$. We will assume that the transition probability is constant in time. In locally homogeneous network dynamics, the transition probabilities can be given by

$$P_{ji} = \frac{1-\mu_i}{d_i}, \tag{1}$$

where d_i is the degree of node i.

Note that as long as only the queue length statistics are concerned and not the fate of individual particles (e.g., trajectories or travel times), the order in which the particles leave the queues is irrelevant. Therefore, individual particles can be considered to be indistinguishable, and not only the first, but any packet can be selected from the queues for delivery.

In each time step, after the delivery or absorption of the existing particles in the system, new particles can also enter the queues randomly. We assume that the probability, p_i, that a new particle enters the system at node i is also constant in time. In addition, we will assume that the queuing system is open, that is particles are generated and absorbed with nonzero probability.

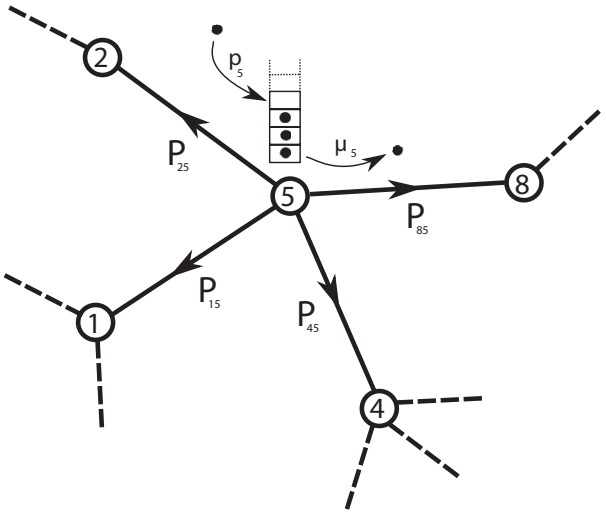

FIG. 1. A schematic figure illustrating the dynamics of the model. Particles are generated and absorbed at node i by probability p_i and μ_i, respectively. The probability that a particle is delivered from node i to node j is denoted by P_{ji}.

The queuing network can be in either a free or a congested state. The network is in free state if, after a transient period, the number of particles in the system fluctuates around an average value. This stationary behavior does not depend on the initial distribution of the length of the queues [18,19]. In this case, the average number of particles arriving to the system equals the average number of particles leaving the network. On the other hand, in the congested state the average number of particles arriving to the system is greater than the average number of particles absorbed. Therefore, in the congested state, the average number of particles in the network will almost surely increase in time. This observation suggests the definition of the order parameter

$$\eta(p_1,\ldots,p_N) = \lim_{t\to\infty} \frac{n(t+1)-n(t)}{\sum_i p_i}, \tag{2}$$

which measures the expected growth rate of the number of particles in the system, $n(t)$, at time t, relative to the arrival rate of incoming particles, $\sum_i p_i$ [4,20–23].

In the case of a stationary state, the order parameter is obviously zero, whereas in the congested state it is greater than zero. The transition between the free and congested states can be characterized by the critical probability, $\mathbf{p}_c = (p_1, p_2, \ldots, p_N)^T$, where the expected arrival rate of the incoming particles equals the expected rate of absorbed particles at least at one of the queues. It has been shown earlier [24,25] that several characteristics of these networks (e.g., probability distribution of delay times, queue length distribution, etc.) show power law dependence on the loading probability near the critical point, which suggests a close analogy with the theory of phase transitions.

III. CONGESTION IN ARBITRARY NETWORKS

In this section we present an analytical estimation of the critical point using a mean-field approximation [15].

Let us suppose first that the queuing system is in equilibrium. In this case, the expected number of particles arriving at each queue is equal to the expected number of particles leaving the queue, that is

$$\xi_i = p_i + \Delta_i, \tag{3}$$

where ξ_i denotes the expected number of particles leaving the queue, Δ_i denotes the expected number of particles arriving to node i from its neighbors in one time step, and p_i is the arrival rate of the particles at node i. Since either zero or one particle leaves the queue in each time step, ξ_i is also equal to the probability that the queue of node i is not empty. Our model is a large-scale Jackson network [18] and it belongs to the class of zero-range processes [26], so the mean-field approximation in the long time limit is exact, the distribution of the queue lengths factorizes on the graph. (For the detailed investigation of the question, see the Appendix of Ref. [15].)

Therefore, Δ_i can be calculated as

$$\Delta_i = \sum_j P_{ij}\xi_j. \tag{4}$$

With standard vector and matrix notations we obtain that in the uncongested, stationary phase the state vector $\boldsymbol{\xi}$ has to satisfy the equation $(\mathbf{E}-\mathbf{P})\boldsymbol{\xi} = \boldsymbol{p}$, where $\mathbf{E}$ denotes the identity matrix. Since the matrix $\mathbf{E}-\mathbf{P}$ is invertible (see Appendix A), the loading probabilities uniquely determine the components of the state vector $\boldsymbol{\xi}$ in the uncongested phase:

$$\boldsymbol{\xi} = (\mathbf{E}-\mathbf{P})^{-1}\boldsymbol{p}. \tag{5}$$

The state of the network can be classified according to the state vector $\boldsymbol{\xi}$. If the components of $\boldsymbol{\xi}$ satisfy the inequality $\xi_i < 1$ for all i, then the network is in an uncongested state, whereas if there is at least one node where $\xi_i = 1$, the network is in the congested state. Therefore, based on this condition, the order parameter of the system can be calculated theoretically.

Note first that the balance Eq. (3) cannot hold at the congested nodes of the network, because the expected number of incoming particles is greater than one, which is the maximum of the expected number of outgoing particles at a queue. Therefore, the congested queues grow steadily, and these queues are never empty. It follows that $\xi_i = 1$ for the congested queues, and the expected growth rate of these queues can be given by $p_i + \Delta_i - 1$. Based on these observations, we can develop an algorithm, presented in Appendix C, that can be used to calculate the order parameter numerically for arbitrary networks and traffic load.

In order to validate our model, we compared the order parameter obtained from our algorithm with packet-level simulations on the same network. For comparison we used the uncorrelated Barabási-Albert (BA) [27], Erdős-Rényi (ER) [28], and Watts-Strogatz (WS) [29] networks. The loading probability was the same at every node of the network, and both the absorption probabilities and the elements of the transition matrix $\mathbf{P}$ were random numbers distributed uniformly between zero and one.

The results are shown in Fig. 2. It can be seen that the theoretical curve, computed by our numerical method, fits very well to the values of the order parameter determined by simulations.

We also validated our results for inhomogeneous traffic loads. For this purpose we generated several realizations of random loading vectors, $\boldsymbol{p}$, and transition matrix $\mathbf{P}$ on the same ER graph and compared the order parameter calculated by simulations and numerical computations. Results are shown in Fig. 3. The simulations agree with our numerical method very well.

IV. CRITICAL TRAFFIC LOAD IN ARBITRARY NETWORKS

The main difficulty of using Eq. (5) is the computational complexity of inverting the matrix $\mathbf{E}-\mathbf{P}$. Moreover, even if the matrix can be inverted numerically for a particular network, the dependence of the critical point on the network structure and the traffic load remains obscure. In the case of large irregular networks, approximations are needed to describe the phase transition analytically.

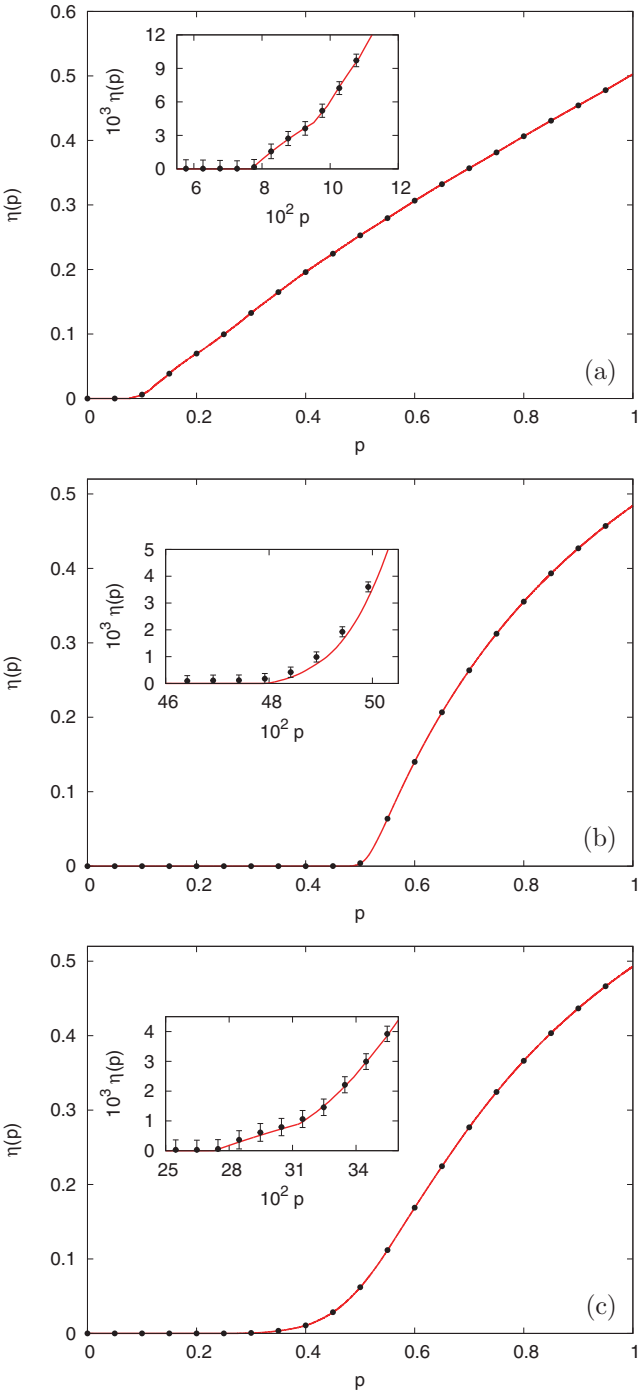

FIG. 2. (Color online) The order parameter as a function of homogeneous loading probabilities. The graphs show numerical calculations (solid line) and particle-based simulations (black points) on three distinct networks. All graphs had $N = 500$ nodes. (a) BA network ($m = 2$); (b) ER network ($p_{\mathrm{ER}} = 0.4$); (c) WS network ($z = 16$ and $q_{\mathrm{WS}} = 0.1024$).

For a detailed analysis of topological effects on the critical load $\boldsymbol{p}_c$, let us consider networks with random-walk-like particle transport with homogeneous absorption probabilities. In this case, if nodes i and j are connected in the network, the transition probability from node i to node j is

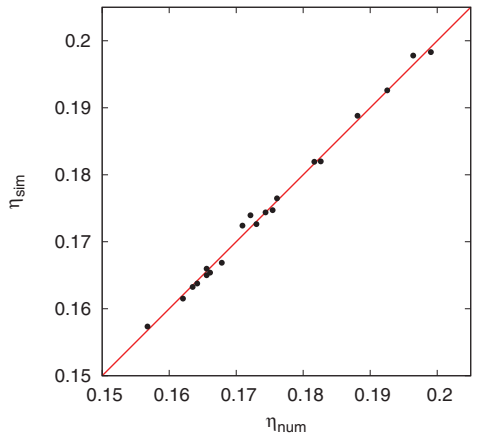

FIG. 3. (Color online) Comparison of the order parameter computed numerically with our algorithm and obtained from simulation with inhomogeneous loading probabilities on an ER graph ($N = 500$ and $p_{ER} = 0.4$).

$P_{ji} = (1-\mu)/d_i$, where d_i is the degree of node i, and μ is the absorption probability. Using the adjacency and degree matrix of the network, $\mathbf{P}$ can be written in a very compact form:

$$\mathbf{P} = (1-\mu)\mathbf{A}\mathbf{D}^{-1}. \tag{6}$$

Using the spectral decomposition of the transition matrix, we can write

$$\mathbf{A}\mathbf{D}^{-1} = \sum_{k=1}^{N} \lambda_k \boldsymbol{v}_k \boldsymbol{w}_k^T, \tag{7}$$

where $\boldsymbol{w}_k$ and $\boldsymbol{v}_k$ are the left and right eigenvectors of $\mathbf{A}\mathbf{D}^{-1}$, respectively, and λ_k is the corresponding eigenvalue. Note that the symmetric matrix $\mathbf{D}^{-1/2}\mathbf{A}\mathbf{D}^{-1/2}$ has the same eigenvalue spectrum as the transition matrix $\mathbf{A}\mathbf{D}^{-1}$. Indeed, if $\boldsymbol{u}_k$ is an eigenvector of the later matrix with eigenvalue λ_k, then $\boldsymbol{v}_k = \mathbf{D}^{1/2}\boldsymbol{u}_k$ will be the right, and $\boldsymbol{w}_k = \mathbf{D}^{-1/2}\boldsymbol{u}_k$ will be the left eigenvector of $\mathbf{A}\mathbf{D}^{-1}$ with the same eigenvalue [30].

The transition matrix $\mathbf{A}\mathbf{D}^{-1}$ is well known in the theory of random walks on graphs [30]. Its eigenvalues satisfy the inequality $-1 \leqslant \lambda_k \leqslant 1$ [30]. The largest eigenvalue is always $\lambda_1 = 1$ and it is degenerate only if the graph is not connected. Moreover, the smallest eigenvalue is equal to -1 if and only if the graph is bipartite [30]. In the following we will assume that the graphs under study are connected.

It is easy to see that the normalized eigenvector of $\mathbf{D}^{-1/2}\mathbf{A}\mathbf{D}^{-1/2}$ corresponding to $\lambda_1 = 1$ is $\boldsymbol{u}_1 = \mathbf{D}^{1/2}\mathbf{1}/\sqrt{2M}$, where M is the number of links in the network, and $\mathbf{1} = (1,1,\ldots,1)^T$. It follows that the left and right eigenvectors of $\mathbf{A}\mathbf{D}^{-1}$ corresponding to $\lambda_1 = 1$ are $\boldsymbol{w}_1 = \mathbf{1}^T/\sqrt{2M}$ and $\boldsymbol{v}_1 = \boldsymbol{d}/\sqrt{2M} = \mathbf{D}\mathbf{1}/\sqrt{2M}$, respectively.

Using the power series expansion of the function $1/(1-x)$ and the spectral decomposition of the transition matrix, we can formally calculate the inverse of $\mathbf{E} - \mathbf{P}$:

$$(\mathbf{E}-\mathbf{P})^{-1} = \sum_{k=1}^{N} \frac{1}{1-(1-\mu)\lambda_k} \boldsymbol{v}_k \boldsymbol{w}_k^T. \tag{8}$$

The above sum can be split into three parts that behave differently as μ varies:

$$\sum_{\lambda_k=0} \boldsymbol{v}_k \boldsymbol{w}_k^T + \frac{1}{\mu}\frac{\boldsymbol{d}\mathbf{1}^T}{2M} + \sum_{\lambda_k\neq 0,1} \frac{1}{1-(1-\mu)\lambda_k} \boldsymbol{v}_k \boldsymbol{w}_k^T. \tag{9}$$

The first term, corresponding to the eigenvalues $\lambda_i = 0$, is independent of μ. The second term, which belongs $\lambda_1 = 1$, becomes singular as $\mu \to 0$. The last term, which consists of all the eigenvalues that are neither zero nor one, is finite for every value of μ.

V. DISCUSSION

A. Low absorption levels

In the case of low absorption levels, the second term dominates in Eq. (9). Therefore, we obtain

$$\boldsymbol{\xi} = (\mathbf{E}-\mathbf{P})^{-1}\,\boldsymbol{p} \simeq \frac{\boldsymbol{d}}{\overline{d}}\frac{\overline{p}}{\mu}, \tag{10}$$

where $\overline{p} = \sum_i p_i/N$ and $\overline{d} = 2M/N$. Moreover, if the loading is homogeneous, i.e., $\boldsymbol{p} = p\mathbf{1}$, the critical loading probability is

$$p_c = \frac{\overline{d}}{d_{\max}}\mu, \tag{11}$$

where $d_{\max}$ is the maximal degree in the graph.

Note that in the low absorption limit the critical point depends only on the relative spread of the degree sequence, i.e., $d_{\max}/\overline{d}$, and not on the absolute scale of the degrees. In particular, in the case of regular graphs, where each node has the same degree, the relative spread is $d_{\max}/\overline{d} = 1$, so the critical point, $p_c = \mu$, is independent of the degree of a regular graph. Furthermore, $d_{\max}$ is always greater than or equal to $\overline{d}$, and equality holds if and only if the graph is regular. Therefore, the critical point p_c is the highest in regular graphs at a given absorption level.

B. High absorption levels

If the absorption probability μ is close to one, then $(1-\mu)\lambda_k$ is close to zero, so the denominators of the third term in Eq. (9) can be approximated by one. Since the eigensystem of $\mathbf{A}\mathbf{D}^{-1}$ is complete, we obtain that

$$(\mathbf{E}-\mathbf{P})^{-1} \simeq \mathbf{E} + \frac{1-\mu}{\mu}\frac{\boldsymbol{d}\mathbf{1}^T}{2M}, \tag{12}$$

and the state vector can be approximated by

$$\boldsymbol{\xi} \simeq \boldsymbol{p} + (1-\mu)\frac{\boldsymbol{d}}{\overline{d}}\frac{\overline{p}}{\mu}. \tag{13}$$

Note that we kept the $1/\mu$ factor in Eq. (13). This way Eq. (13) can reproduce Eq. (10) in the small absorption limit, since $\boldsymbol{p}$ can be neglected compared to the second term, which diverges if $\mu \to 0$.

In the case of homogeneous loading, the critical loading probability is

$$p_c \simeq \frac{\mu}{\mu + (1-\mu)d_{\max}/\overline{d}}, \tag{14}$$

which depends again only on $d_{\max}/\overline{d}$, the relative spread of the degree sequence. It is remarkable that the critical point is almost completely independent of the fine details of the network structure in both the small and high absorption limit.

C. Intermediate absorption levels

Numerical simulations presented later in this section show that Eq. (13) is valid not only for small and large values of μ but also for intermediate values if the edge density of the graph is large. The reasons are the following. The approximation that leads to Eq. (13) is the assumption that the term $(1-\mu)\lambda_k$ is close to zero for those λ_k, that are neither equal to zero nor one. This approximation is valid not only when μ is close to one, but also if the second largest absolute eigenvalue is close to zero.

If the graph is nonbipartite, the second largest absolute eigenvalue is related to τ, the characteristic time until a particle reaches the stationary distribution of a random walk, as $1/\tau = \max\{|\lambda_2|, |\lambda_N|\}$. Numerical calculations, presented in Sec. V D, show that $1/\tau$ decreases when the average degree increases and remains constant with small fluctuations if the average degree is fixed. Therefore, in the case of dense networks, it is plausible to use the lowest terms of the power series expansion

$$\frac{1}{1-(1-\mu)\lambda_k} = 1 + (1-\mu)\lambda_k + (1-\mu)^2\lambda_k^2 + \cdots . \quad (15)$$

in the third term of Eq. (9). The zeroth-order term of the series expansion reproduces Eq. (13). If the network is not dense, like many real networks, or the absorption level is in the intermediate range, we need to consider the first-order term in the power series expansion Eq. (15) as well. Since bipartite and nonbipartite graphs are qualitatively different, we will discuss the two cases separately.

1. Nonbipartite graphs

It is easy to see that the first-order correction to $(\mathbf{E}-\mathbf{P})^{-1}$ is $(1-\mu)(\mathbf{A}\mathbf{D}^{-1} - \boldsymbol{d}\mathbf{1}^T/2M)$. Using this correction we obtain that the state vector can be approximated by

$$\boldsymbol{\xi} \simeq \boldsymbol{p} + (1-\mu)\mathbf{A}\mathbf{D}^{-1}\boldsymbol{p} + (1-\mu)^2\frac{\boldsymbol{d}}{\overline{d}}\frac{\overline{p}}{\mu}. \quad (16)$$

In order to study the effects of the topology on the critical traffic load, let us consider homogeneous loading probabilities. After straightforward calculations, we obtain that in this case the ith component of the state vector is

$$\frac{\xi_i}{p} \simeq 1 + \frac{(1-\mu)^2}{\mu}\frac{d_i}{\overline{d}} + (1-\mu)\frac{d_i}{h_i}, \quad (17)$$

where h_i denotes the harmonic mean of the degree of the neighbors of the ith node,

$$h_i = \left(\frac{1}{d_i}\sum_{j\in\mathcal{N}(i)}\frac{1}{d_j}\right)^{-1}, \quad (18)$$

and $\mathcal{N}(i)$ is the set of neighbors of node i. Consequently, we obtain that the critical loading probability is

$$\frac{1}{p_c} \simeq 1 + \max_i\left\{\frac{(1-\mu)^2}{\mu}\frac{d_i}{\overline{d}} + (1-\mu)\frac{d_i}{h_i}\right\}, \quad (19)$$

which is one of the main results of our paper.

The main novelty of Eq. (19) is that it shows that the critical point of the phase transition is determined not only by the spread of the degree sequence, $d_{\max}/\overline{d}$, like in the low and high absorption limit, but also by h_i, which depends on the local structure of the network.

We validated our result on BA and ER networks. We calculated the critical load p_c by inverting Eq. (5) numerically and then compared the result with Eq. (14) and Eq. (19) on the same graph with the same absorption level.

The results are presented in Fig. 4. It can be seen that the zeroth-order approximation (14) is valid only for small and large absorption levels. On the contrary, the first-order approximation (19) fits the numerical data closely on the whole range of absorption levels. In order to emphasize the clear advantage of Eq. (19), the absolute difference between Eqs. (14) and (19) and the numerical data is also shown in Fig. 4.

2. Bipartite graphs

The nodes of a bipartite graph can be divided into two disjoint groups, $\mathcal{G}_1$ and $\mathcal{G}_2$, in such a way that the edges of the graph connect only nodes from different groups. Since trees are bipartite graphs, bipartite graphs are extremely important from the practical point of view.

Suppose that there are N_1 nodes in $\mathcal{G}_1$ and N_2 nodes in $\mathcal{G}_2$, and denote the average degree and loading probability in $\mathcal{G}_i$ $(i = 1,2)$ are $\overline{d}_i = M/N_i$ and $\overline{p}_i = \sum_{k\in\mathcal{G}_i} p_k/N$, respectively.

The critical traffic load in bipartite graphs can be calculated similarly to the nonbipartite graphs. The calculation is based on the symmetry of the spectra of the transition matrix. Here, we only summarize the results for homogeneous loading, details of the calculation and the case of heterogeneous loading are presented in Appendix B.

In the case of a bipartite graph, we obtain that each partition defines a separate critical loading probability. For low or high absorption levels and homogeneous traffic load we obtain, analogously to Eq. (14), that

$$\begin{aligned}\frac{1}{p_c^{(1)}} &\simeq 1 + \frac{1}{\mu}\frac{(1-\mu)^2/\overline{d}_1 + (1-\mu)/\overline{d}_2}{2-\mu}d_{\max}^{(1)},\\ \frac{1}{p_c^{(2)}} &\simeq 1 + \frac{1}{\mu}\frac{(1-\mu)^2/\overline{d}_2 + (1-\mu)/\overline{d}_1}{2-\mu}d_{\max}^{(2)},\end{aligned} \quad (20)$$

where $d_{\max}^{(i)}$ is the maximal degree in $\mathcal{G}_i$. The critical loading probability of the whole network is the lesser of the two: $p_c = \min(p_c^{(1)}, p_c^{(2)})$.

This result is very similar to the case of nonbipartite graphs. It can be seen that p_c depends only on the absorption level, μ, and global properties of the graph, namely the mean $\overline{d}_i$ and the maximal degree $d_{\max}^{(i)}$, which can be obtained from the degree sequences of $\mathcal{G}_1$ and $\mathcal{G}_2$ straightforwardly.

In the case of intermediate absorption levels, the zeroth-order approximation of critical traffic load, presented in Eq. (20), has to be corrected. Similar to nonbipartite

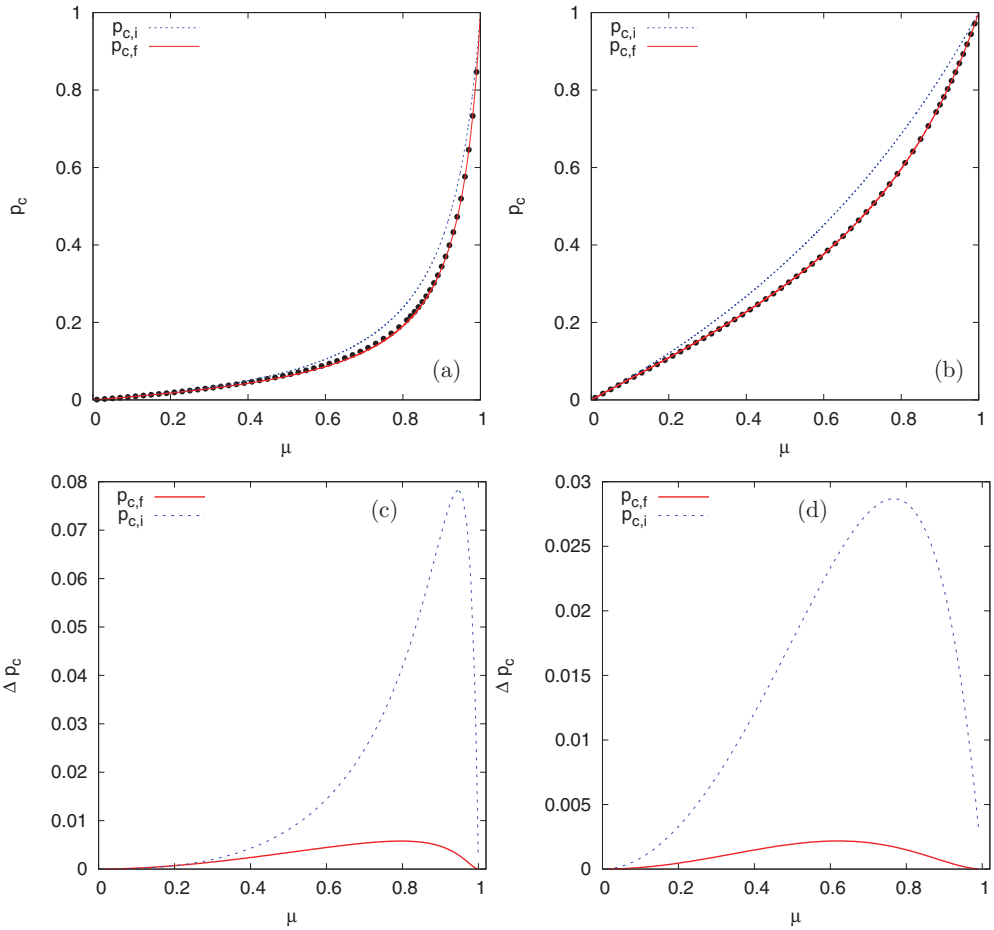

FIG. 4. (Color online) Numerical validation of the analytic results in BA ($N = 512$ nodes, $m = 2$) and ER ($N = 64$ nodes, $p = 0.1$) networks. The dashed and continuous lines $p_{c,i}$ and $p_{c,f}$ represent Eqs. (14) and (19), respectively. Numerical data, obtained by solving Eq. (5) numerically, are represented by dots. (a) The critical load, p_c, in a BA network; (b) the critical load, p_c, in an ER network; (c) The absolute error, Δp_c, in a BA network; (d) The absolute error, Δp_c, in an ER network.

graphs, the first-order correction, obtained from the spectral decomposition of the transition matrix, is proportional to d_i/h_i. The critical loading probabilities $p_c^{(1)}$ and $p_c^{(2)}$, including the first-order corrections and corresponding to the two subcomponents of a bipartite graph, are

$$\begin{aligned}\frac{1}{p_c^{(1)}} &\simeq 1 + \max_{i\in\mathcal{G}_1}\left\{\frac{1}{\mu}\frac{(1-\mu)^2/\overline{d}_1 + (1-\mu)^3/\overline{d}_2}{2-\mu}d_i \right.\\ &\qquad \left. + (1-\mu)d_i/h_i\right\},\\ \frac{1}{p_c^{(2)}} &\simeq 1 + \max_{i\in\mathcal{G}_2}\left\{\frac{1}{\mu}\frac{(1-\mu)^2/\overline{d}_2 + (1-\mu)^3/\overline{d}_1}{2-\mu}d_i \right.\\ &\qquad \left. + (1-\mu)d_i/h_i\right\}.\end{aligned} \tag{21}$$

Consequently, the critical loading probability of the whole network is $p_c = \min(p_c^{(1)}, p_c^{(2)})$.

In order to validate our results, we calculated the critical load p_c by inverting Eq. (5) numerically. For validation, we used BA scale-free trees, grown by preferential attachment, and compared the numerical data with Eqs. (20) and (21) with the same graph and absorption level. The results are shown in Fig. 5. Equation (21), which includes first-order corrections, fits the numerical data closely, not only at low and high absorption levels, like Eq. (20), but also in the intermediate absorption range.

D. Error estimation in the large graph limit

We have seen that in the case of nonbipartite graphs the largest absolute eigenvalue is $|\lambda_1| = 1$, whereas in case of bipartite graphs it is $|\lambda_1| = |\lambda_N| = 1$. In the power series expansion Eq. (15) we considered the largest absolute eigenvalue precisely and neglected the higher order terms for $|\lambda| < 1$. In this section we discuss the validity of our approximation and show numerically how the precision of our model depends on the graph properties.

The error of the derived formulas depends on the magnitude of the higher-order terms that we neglected in the power series expansion Eq. (15). These terms can be bounded from above with the second-largest absolute eigenvalue, that is $\max\{|\lambda_2|, |\lambda_N|\}$ for nonbipartite graphs and λ_2 for bipartite graphs. The smaller the second largest absolute eigenvalues are, the smaller the error of Eq. (19) and Eq. (21) is.

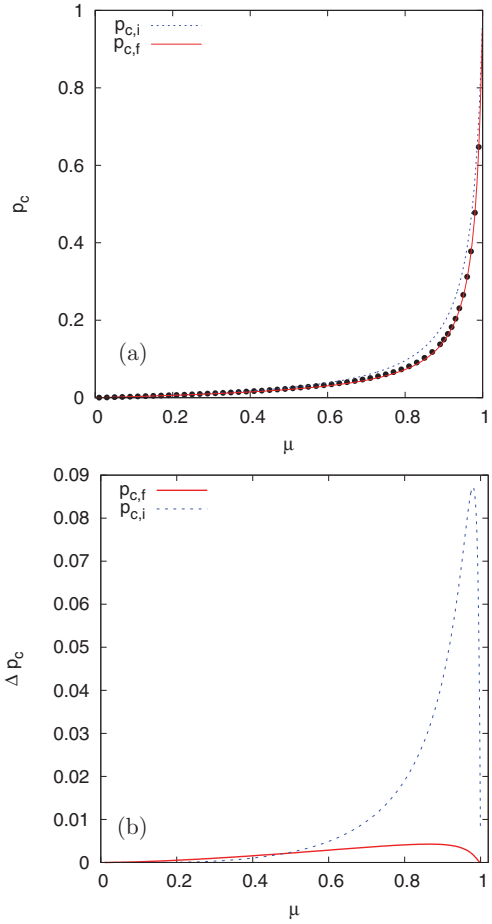

FIG. 5. (Color online) Numerical validation of the analytic results on a BA tree ($N = 1024$ nodes, $m = 1$). The dashed and continuous lines $p_{c,i}$ and $p_{c,f}$ represent Eqs. (20) and (21), respectively. Numerical data, obtained by solving Eq. (5) numerically, are represented by dots. (a) The critical load, p_c, as a function of the absorption level, μ; (b) the absolute error of the critical load, Δp_c, as a function of the absorption level, μ.

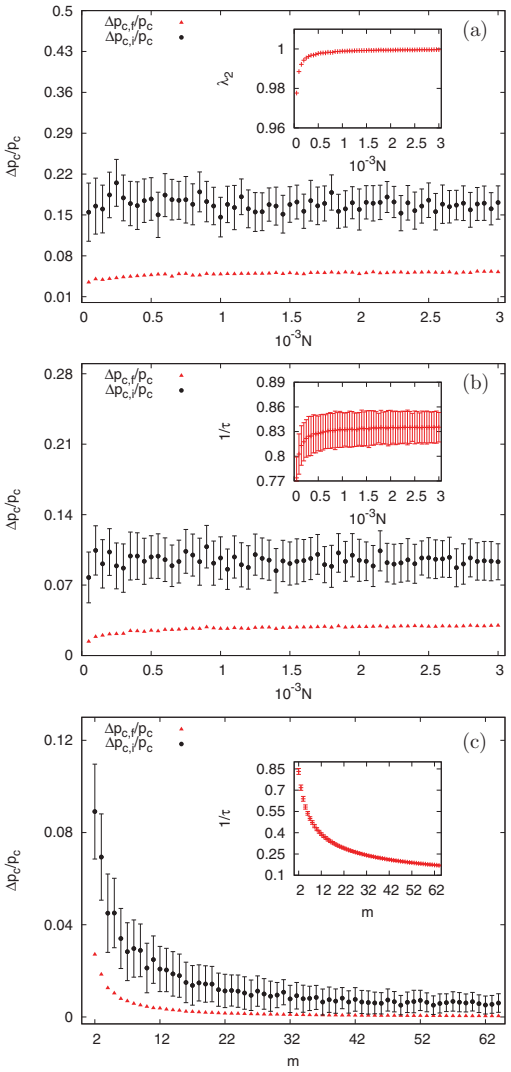

FIG. 6. (Color online) The relative error, $\Delta p_c/p_c$, of the derived formulas as a function of N and m in BA networks with absorption rate $\mu = 0.8$. The black dots and red triangles show the error of the derived zeroth- and first-order approximations, respectively. The insets show the dependence of the mixing rate, $1/\tau$, on N and m. Data points were averaged over 32 graph realization in each case. (a) BA tree with $m = 1$ fixed and N varied; (b) BA network with $m = 2$ fixed and N varied; (c) BA network with $N = 1024$ fixed and m varied.

Although it is easy to manipulate the eigenvalues λ_k formally, it is difficult to see how the eigenvalues depend on the graph properties. In order to see more easily how the error depends on the graph properties, let us introduce the mixing time from the theory of random walk on graphs.

The mixing time, τ, is the expected time until a particle, performing random walk on a graph, reaches a stationary distribution. It can be shown that the mixing rate, the reciprocal of the mixing time, is precisely equal to the second largest eigenvalue, i.e., $1/\tau = \max\{|\lambda_2|, |\lambda_N|\}$ for nonbipartite graphs and $1/\tau = \lambda_2$ for bipartite graphs [30]. Therefore, it is plausible to conclude that for graphs that have small mixing rate, the error will be also small.

There is no known formula in the literature on how the mixing rate depends on the graph parameters in general [31]. However, our numerical experiments showed that the mixing rate depends strongly on the edge density, $M/N = \overline{d}/2$. In particular, the mixing rate decreases as the edge density increases. In Fig. 7 we can see the relative error of the derived formulas, $\Delta p_c/p_c$, as the function of various graph parameters. In the inset we can see the mixing rate as the function of the corresponding graph parameter.

In the case of a BA network, for example , the edge density is $M/N \simeq m$, where m is the number of edges connecting the new nodes to the graph in preferential attachment. This means that the mixing rate, $1/\tau$, remains constant with small fluctuations if m is fixed, even if $N \to \infty$. This phenomenon is the same in bipartite and nonbipartite graphs. For example, one obtains a BA scale-free tree, which is a bipartite graph, if $m \equiv 1$, In this case, the error of the derived formulas is also constant, and it will not decrease even in the thermodynamic limit.

In Fig. 6(a) and Fig. 6(b) we can see BA networks with $m = 1$ and $m = 2$ fixed, and N varied. These cases correspond

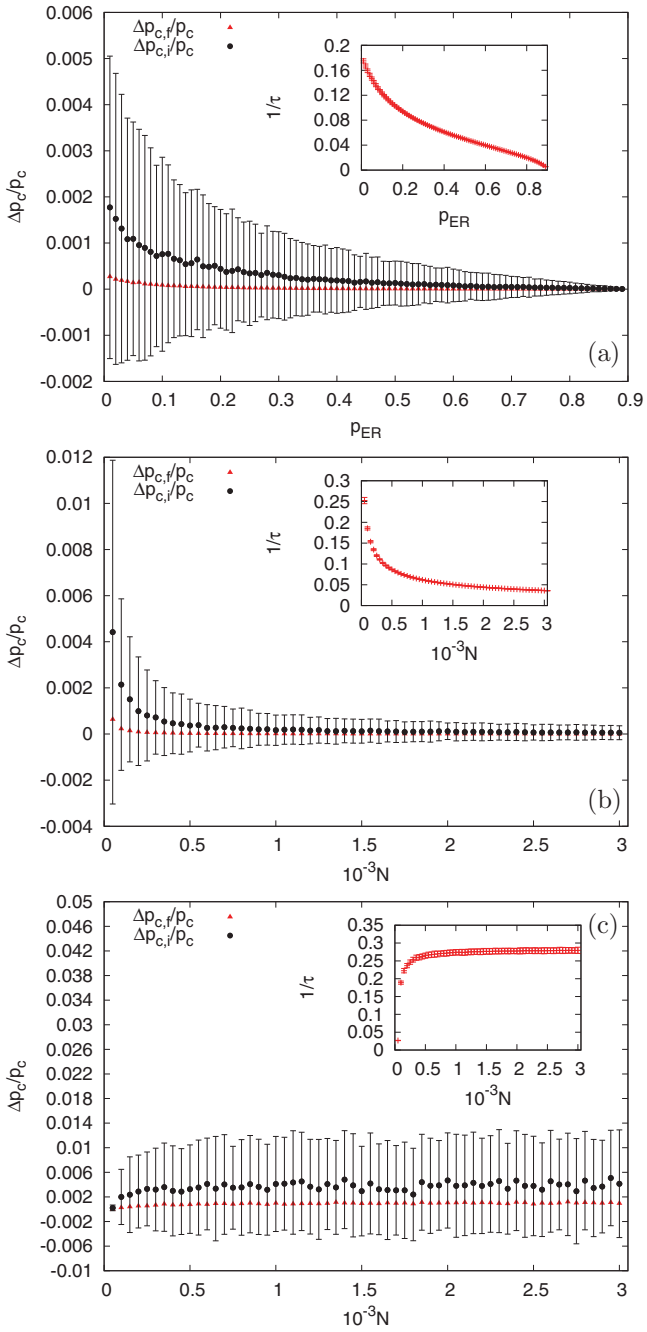

FIG. 7. (Color online) The relative error, $\Delta p_c/p_c$, of the derived formulas as a function of N and p_{ER} in ER networks with absorption rate $\mu = 0.8$ (Figs. 7(a) and 7(b)) and $\mu = 0.5$ (Fig. 7(c)). The black points and red triangles show the error of the derived zeroth and first order approximation, respectively. The insets show the dependence of the mixing rate, $1/\tau$, on N and p_{ER}. Data points were averaged over 32 graph realizations in each case. (a) ER network with $N = 1024$ fixed and p_{ER} varied; (b) ER network with $p_{\mathrm{ER}} = 0.5$ fixed and N varied; (c) ER with $Np_{\mathrm{ER}} = 49$ fixed, N and p_{ER} varied.

to a bipartite and a nonbipartite graph, respectively. We can see that in both cases both the relative error and the mixing rate tends to a fixed value as $N \to \infty$. On the other hand, in Fig. 6(c) the size of the graph is fixed, and m is varied. We can see that the mixing rate increases as m increases and, at the same time, the relative tends to zero.

The construction of ER networks is fundamentally different from the BA graphs. In the case of ER networks, the edge density is $M/N = p(N-1)/2 \simeq pN/2$. Therefore, the edge density increases, and the relative error tends to zero, if either p or N is increased, and the other parameter is fixed. Note that in the case of $p = 1$ the ER network is a complete graph, in which case the derived formulas are exact. In contrast, the relative error of the derived formulas tends to a fixed value if pN is fixed.

Numerical simulations carried out on ER networks are shown in Fig. 7. We can see that the simulation results confirm our assumption that the relative error of the derived formulas decreases if the density of the network increases and remain fixed if the density is fixed.

VI. CONCLUSION

In this paper, we studied congestion phenomena in queuing networks. We analyzed how the critical point of the phase transition between free and congested phases is influenced by the topological properties of the network. In order to study the influence of the network structure on the traffic dynamics in an arbitrary network, we neglected congestion control mechanisms, and we modeled the particle transport by a simple Markovian random walk.

In our model the critical traffic load in the network can be controlled by the absorption level of the particles. We first derived Eq. (14), the zeroth-order approximation for the critical traffic load for low and high absorption levels. For high absorption levels, our formulas are the same on quenched networks as the results of De Martino *et al.* [15] on a model with a congestion control mechanism included on annealed networks. Our result extends their finding that at the critical point the details of the congestion control mechanism are less important in some cases of networks with quenched disorder.

In our paper we also showed that in the case of intermediate absorption levels the zeroth-order formula is not valid, and higher-order corrections are needed. We derived Eq. (19), which incorporates the first-order corrections to Eq. (14) and improves the precision of the critical point considerably. In contrast to the zeroth-order formula, higher-order corrections include not only the global properties of the degree sequence, i.e., the mean and maximum degree, but also the local information on the network structure. The improvement achieved by the higher-order correction was validated by numerical simulations.

We also demonstrated that in the case of intermediate absorption levels the structure of the network can have dramatic effects on the analytic behavior of the critical point. We showed, in particular, that one must pay special attention when considering a bipartite graph, because the spectra of bipartite graphs are symmetrical. We derived Eq. (21) and showed that the critical point in a bipartite graph is the maximum of the critical points of its subcomponents.

Finally, we investigated the validity of our model. We showed that the higher-order terms that were neglected during our calculations depend on the spectral gap, which can also be expressed by the mixing rate in the graph. We presented

numerical arguments that the mixing ratio, that is the precision of our approximations, strongly depends on the edge density M/N. This empirical fact is well known in the mathematical community, but up to now, as far as we know, there is no rigorous proof of the phenomenon. We would like to examine this question in detail in our future work.

ACKNOWLEDGMENTS

This work was partially supported by the National Science Foundation OTKA 7779, the National Development Agency (TAMOP 4.2.1/B-09/1/KMR-2010-0003), and the EU FIRE NOVI project (Grant No. 257867). We are also grateful to László Lovász for the useful discussions on the mixing rate of graphs.

APPENDIX A

Let us suppose that $\mathbf{E}-\mathbf{P}$ is not invertible, which is equivalent to the statement that $\mathbf{P}$ has a normalized eigenvector $\boldsymbol{x}$ with eigenvalue 1. In this case, using the assumption that there is at least one node where $\sum_i P_{ij} < 1$ (i.e., there is absorption at least at one node), the following inequalities will hold:

$$\sum_{i=1}^{N}|x_i| \leqslant \sum_{j=1}^{N}\sum_{i=1}^{N} P_{ij}|x_j| < \sum_{j=1}^{N}|x_j|, \tag{A1}$$

which is a contradiction.

APPENDIX B

Using an indexing of the nodes that is suitable for the definition of bipartite graphs, every vector mentioned in the main text can be split into two parts, $\boldsymbol{p}=(\boldsymbol{p}_1,\boldsymbol{p}_2)^T$, $\boldsymbol{d}=(\boldsymbol{d}_1,\boldsymbol{d}_2)^T$ $\boldsymbol{\xi}=(\boldsymbol{\xi}_1,\boldsymbol{\xi}_2)^T$, such that the N_1 (N_2) components of the first (second) part belong to nodes in $\mathcal{G}_1$ ($\mathcal{G}_2$). The form of $\mathbf{A}$ and $\mathbf{D}$ are the following.

$$\mathbf{A}=\begin{pmatrix}\mathbf{0} & \mathbf{B}\\ \mathbf{B}^T & \mathbf{0}\end{pmatrix} \quad \mathbf{D}=\begin{pmatrix}\mathbf{D}_1 & \mathbf{0}\\ \mathbf{0} & \mathbf{D}_2\end{pmatrix}, \tag{B1}$$

where $\mathbf{B}$ is an $N_1\times N_2$, $\mathbf{D}_1$ is an $N_1\times N_1$, and $\mathbf{D}_2$ is an $N_2\times N_2$ matrix. The transition matrix has the following form:

$$\mathbf{AD}^{-1}=\begin{pmatrix}\mathbf{0} & \mathbf{B}\mathbf{D}_2^{-1}\\ \mathbf{B}^T\mathbf{D}_1^{-1} & \mathbf{0}\end{pmatrix}. \tag{B2}$$

The structure of $\mathbf{D}^{-1/2}\mathbf{A}\mathbf{D}^{-1/2}$ is similar to $\mathbf{A}$, the off-diagonal block matrices are $\mathbf{D}_1^{-1/2}\mathbf{B}\mathbf{D}_2^{-1/2}$ and its transpose. A one-line calculation shows that if $\boldsymbol{u}_i=(\boldsymbol{u}_{1,k},\boldsymbol{u}_{2,k})^T$ is an eigenvector of $\mathbf{D}^{-1/2}\mathbf{A}\mathbf{D}^{-1/2}$ with eigenvalue λ_k, then the vector $(\boldsymbol{u}_{1,k},-\boldsymbol{u}_{2,k})^T$ is also an eigenvector with eigenvalue $-\lambda_k$, so the spectra of $\mathbf{D}^{-1/2}\mathbf{A}\mathbf{D}^{-1/2}$ is symmetric to the origin. One consequence of this symmetry is that if the number of nodes is even (odd), the kernel dimension of $\mathbf{D}^{-1/2}\mathbf{A}\mathbf{D}^{-1/2}$ is also even (odd). For the sake of simplicity, we study only bipartite graphs with an even number of nodes. For large networks, this has no serious consequence. Let us define the matrices $\mathbf{I}_k^{(1)}$ and $\mathbf{I}_k^{(2)}$:

$$\mathbf{I}_k^{(1)}=\begin{pmatrix}\boldsymbol{u}_{1,k}\boldsymbol{u}_{1,k}^T & \mathbf{0}\\ \mathbf{0} & \boldsymbol{u}_{2,k}\boldsymbol{u}_{2,k}^T\end{pmatrix}, \tag{B3}$$

and

$$\mathbf{I}_k^{(2)}=\begin{pmatrix}\mathbf{0} & \boldsymbol{u}_{1,k}\boldsymbol{u}_{2,k}^T\\ \boldsymbol{u}_{2,k}\boldsymbol{u}_{1,k}^T & \mathbf{0}\end{pmatrix}. \tag{B4}$$

Then, the spectral decomposition of $\mathbf{D}^{-1/2}\mathbf{A}\mathbf{D}^{-1/2}$ is

$$\sum_{k=1}^{N}\lambda_k\left(\mathbf{I}_k^{(1)}+\mathbf{I}_k^{(2)}\right)=\sum_{k=1}^{N/2}2\lambda_k\mathbf{I}_k^{(2)}. \tag{B5}$$

It is easier to perform the calculation on the spectral decomposition of $\mathbf{D}^{-1/2}\mathbf{A}\mathbf{D}^{-1/2}$ instead of $\mathbf{A}\mathbf{D}^{-1}$ to get an approximation of $(\mathbf{E}-\mathbf{P})^{-1}$:

$$(\mathbf{E}-\mathbf{P})^{-1}=\mathbf{D}^{1/2}[\mathbf{E}-(1-\mu)\mathbf{D}^{-1/2}\mathbf{A}\mathbf{D}^{-1/2}]^{-1}\mathbf{D}^{-1/2}. \tag{B6}$$

The spectral decomposition of the factor in the middle of the right-hand side is

$$\sum_{k=1}^{N}\frac{\boldsymbol{u}_k\boldsymbol{u}_k^T}{1-(1-\mu)\lambda_i}, \tag{B7}$$

which, using the symmetry of the spectra, can be written in the form

$$\sum_{k=1}^{N/2}2\frac{\mathbf{I}_k^{(1)}+(1-\mu)\lambda_k\mathbf{I}_k^{(2)}}{1-(1-\mu)^2\lambda_k^2}. \tag{B8}$$

This also can be split into three parts as in Eq. (9):

$$\sum_{\lambda_k=0}2\mathbf{I}_k^{(1)}+\frac{2}{\mu}\frac{\mathbf{I}_k^{(1)}+(1-\mu)\mathbf{I}_k^{(2)}}{2-\mu} + \sum_{\lambda_k\neq 0,1}2\frac{\mathbf{I}_k^{(1)}+(1-\mu)\lambda_k\mathbf{I}_k^{(2)}}{1-(1-\mu)^2\lambda_k^2}, \tag{B9}$$

but here, summation runs over only the first half of the spectra. The power series expansion of the summands of the last term is

$$2\mathbf{I}_k^{(1)}+2(1-\mu)\lambda_k\mathbf{I}_k^{(2)}+2(1-\mu)^2\lambda_k^2\mathbf{I}_k^{(1)}+\cdots \tag{B10}$$

Dropping all the terms except the first gives

$$\mathbf{E}+\frac{2}{\mu}\frac{(1-\mu)^2\mathbf{I}_1^{(1)}+(1-\mu)\mathbf{I}_1^{(2)}}{2-\mu} \tag{B11}$$

as the inverse of $\mathbf{E}-(1-\mu)\mathbf{D}^{-1/2}\mathbf{A}\mathbf{D}^{-1/2}$, so

$$(\mathbf{E}-\mathbf{P})^{-1}\simeq\mathbf{E}+\frac{1}{\mu}\frac{(1-\mu)^2\mathbf{J}_1^{(1)}+(1-\mu)\mathbf{J}_1^{(2)}}{2-\mu}, \tag{B12}$$

where $\mathbf{J}_1^{(1)}$ and $\mathbf{J}_1^{(2)}$ are the following matrices:

$$\mathbf{J}_1^{(1)}=\frac{1}{M}\begin{pmatrix}\boldsymbol{d}_1\mathbf{1}_1^T & \mathbf{0}\\ \mathbf{0} & \boldsymbol{d}_2\mathbf{1}_2^T\end{pmatrix}, \tag{B13}$$

and

$$\mathbf{J}_1^{(2)}=\frac{1}{M}\begin{pmatrix}\mathbf{0} & \boldsymbol{d}_1\mathbf{1}_2^T\\ \boldsymbol{d}_2\mathbf{1}_1^T & \mathbf{0}\end{pmatrix}. \tag{B14}$$

This gives the values of $\boldsymbol{\xi}_1$ and $\boldsymbol{\xi}_2$:

$$\begin{aligned}\boldsymbol{\xi}_1 &= \boldsymbol{p}_1 + \frac{1}{\mu}\frac{(1-\mu)^2\overline{p}_1/\overline{d}_1 + (1-\mu)\overline{p}_2/\overline{d}_2}{2-\mu}\boldsymbol{d}_1,\\ \boldsymbol{\xi}_2 &= \boldsymbol{p}_2 + \frac{1}{\mu}\frac{(1-\mu)^2\overline{p}_2/\overline{d}_2 + (1-\mu)\overline{p}_1/\overline{d}_1}{2-\mu}\boldsymbol{d}_2.\end{aligned} \tag{B15}$$

Equation (20) gives the final result for homogeneous loading.

To get the first finite-size correction, we have to use not only the first but also the second term in Eq. (B10). Using Eq. (B5), the correction term to the inverse of $\mathbf{E} - (1-\mu)\mathbf{D}^{-1/2}\mathbf{A}\mathbf{D}^{-1/2}$ appears to be $(1-\mu)\mathbf{D}^{-1/2}\mathbf{A}\mathbf{D}^{-1/2} - 2(1-\mu)\mathbf{I}_1^{(2)}$, so the corrected formula for the inverse is

$$\begin{aligned}&\mathbf{E} + \frac{2}{\mu}\frac{(1-\mu)^2\mathbf{I}_1^{(1)} + (1-\mu)^3\mathbf{I}_1^{(2)}}{2-\mu}\\ &\quad + (1-\mu)\mathbf{D}^{-1/2}\mathbf{A}\mathbf{D}^{-1/2},\end{aligned} \tag{B16}$$

and the inverse of $\mathbf{E} - \mathbf{P}$ is

$$\begin{aligned}(\mathbf{E}-\mathbf{P})^{-1} \simeq \mathbf{E} &+ \frac{1}{\mu}\frac{(1-\mu)^2\mathbf{J}_1^{(1)} + (1-\mu)^3\mathbf{J}_1^{(2)}}{2-\mu}\\ &+ (1-\mu)\mathbf{A}\mathbf{D}^{-1}.\end{aligned} \tag{B17}$$

The corrected values of $\boldsymbol{\xi}_1$ and $\boldsymbol{\xi}_2$ are

$$\begin{aligned}\boldsymbol{\xi}_1 &\simeq \boldsymbol{p}_1 + \frac{1}{\mu}\frac{(1-\mu)^2\overline{p}_1/\overline{d}_1 + (1-\mu)^3\overline{p}_2/\overline{d}_2}{2-\mu}\boldsymbol{d}_1\\ &\quad + (1-\mu)\mathbf{B}\mathbf{D}_2^{-1}\mathbf{1}_1\\ \boldsymbol{\xi}_2 &\simeq \boldsymbol{p}_2 + \frac{1}{\mu}\frac{(1-\mu)^2\overline{p}_2/\overline{d}_2 + (1-\mu)^3\overline{p}_1/\overline{d}_1}{2-\mu}\boldsymbol{d}_2\\ &\quad + (1-\mu)\mathbf{B}^T\mathbf{D}_1^{-1}\mathbf{1}_2.\end{aligned} \tag{B18}$$

In the case of homogeneous loading probabilities, this leads to the appearance of the harmonic means:

$$\begin{aligned}\frac{\xi_{1,i}}{p} &\simeq 1 + \frac{1}{\mu}\frac{(1-\mu)^2/\overline{d}_1 + (1-\mu)^3/\overline{d}_2}{2-\mu}\\ &\quad + (1-\mu)d_i/h_i,\\ \frac{\xi_{2,i}}{p} &\simeq 1 + \frac{1}{\mu}\frac{(1-\mu)^2/\overline{d}_2 + (1-\mu)^3/\overline{d}_1}{2-\mu}d_i\\ &\quad + (1-\mu)d_i/h_i,\end{aligned} \tag{B19}$$

and the individual critical loading probabilities in $\mathcal{G}_1$ and $\mathcal{G}_2$ are those that are in Eq. (21).

APPENDIX C

The following algorithm calculates the order parameter. Suppose that $\boldsymbol{p} = p\boldsymbol{e}$, where $\boldsymbol{e}$ is a normalized vector. If p is close to zero, the network is in the uncongested phase, the components of $\boldsymbol{\xi}(p)$ satisfy Eq. (5) and the number of the uncongested nodes is equal to the number of the nodes in the system. If one increases p slowly, one finds that one or more nodes will surely have at least one waiting particle in their queues in the stationary regime, i.e., at least one $\xi_i(p)$ becomes 1 at a certain value of p. Increasing p toward this value drives these nodes to the congested state, and the expected value of the growing length at the queues at these nodes in one time step is $pe_i + \sum_j P_{ij} - 1$. On the other hand, these congested nodes send particles to their neighbors with rates equal to the corresponding element of $\mathbf{P}$. These ideas suggest the following algorithm.

(1) Set $\mathbf{P}^{(0)} = \mathbf{P}$, $\boldsymbol{y}^{(0)} = \boldsymbol{e}$, $z^{(0)} = \mathbf{0}$, and s to a small positive number.

(2) In the kth step, calculate the vector

$$\boldsymbol{x}^{(k)}(s) = (\mathbf{E}^{(k)} - \mathbf{P}^{(k)})^{-1}(s\,\boldsymbol{y}^{(k)} + \boldsymbol{z}^{(k)}). \tag{C1}$$

Starting from the last value at the $(k-1)$th step, increase s until one of the components of $\boldsymbol{x}^{(k)}$ becomes 1, or s becomes p. If the latter is the case, equate the components of $\boldsymbol{\xi}$ to the corresponding components of $\boldsymbol{x}^{(k)}$. If the former is true, set $\xi_i = 1$ at the node where $x_i^{(k)}$ is equal to one—this is the new congested node. Increase every component of $\boldsymbol{z}^{(k)}$ with the corresponding element of $\mathbf{P}$ located in the column of the new congested node. Delete the rows and columns of the new congested node in $\mathbf{E}^{(k)}$, $\mathbf{P}^{(k)}$, $\boldsymbol{x}^{(k)}$, and $\boldsymbol{z}^{(k)}$. This gives matrices $\mathbf{E}^{(k+1)}$, $\mathbf{P}^{(k+1)}$, and vectors $\boldsymbol{x}^{(k+1)}$ and $\boldsymbol{z}^{(k+1)}$ for the $(k+1)$th step.

(3) If all components of $\boldsymbol{\xi}$ are calculated, the order parameter is

$$\eta(\boldsymbol{p}) = \frac{\sum_{\xi_i=1}\left(p_i + \sum_j P_{ij}\xi_j - 1\right)}{\sum_i p_i}. \tag{C2}$$

[1] R. Albert and A.-L. Barabási, Rev. Mod. Phys. **74**, 47 (2002).
[2] M. Newman, SIAM Rev. **45**, 167 (2003).
[3] T. Ohira and R. Sawatari, Phys. Rev. E **58**, 193 (1998).
[4] A. Arenas, A. Díaz-Guilera, and R. Guimerà, Phys. Rev. Lett. **86**, 3196 (2001).
[5] L. Zhao, Y.-C. Lai, K. Park, and N. Ye, Phys. Rev. E **71**, 026125 (2005).
[6] P. Echenique, J. Gómez-Gardeñes, and Y. Moreno, Europhys. Lett. **71**, 325 (2005).
[7] S. Meloni and J. Gómez-Gardeñes, Phys. Rev. E **82**, 056105 (2010).
[8] X. Ling, M.-B. Hu, R. Jiang, R. Wang, X.-B. Cao, and Q.-S. Wu, Phys. Rev. E **80**, 066110 (2009).
[9] X. Ling, M.-B. Hu, R. Jiang, and Q.-S. Wu, Phys. Rev. E **81**, 016113 (2010).
[10] A. Tretyakov, H. Takayasu, and M. Takayasu, Physica A **253**, 315 (1998).
[11] S. H. Strogatz, Nature (London) **410**, 268 (2001).
[12] S. N. Dorogovtsev, A. V. Goltsev, and J. F. F. Mendes, Rev. Mod. Phys. **80**, 1275 (2008).
[13] S. Boccaletti, V. Latora, Y. Moreno, M. Chavez, and D.-U. Hwang, Phys. Rep. **424**, 175 (2006).
[14] G. Mukherjee and S. S. Manna, Phys. Rev. E **71**, 066108 (2005).
[15] D. De Martino, L. Dall'Asta, G. Bianconi, and M. Marsili, J. Stat. Mech. (2009) P08023.

[16] D. De Martino, L. Dall'Asta, G. Bianconi, and M. Marsili, Phys. Rev. E **79**, 015101 (2009).
[17] F. R. K. Chung, *Spectral Graph Theory* (American Mathematical Society, Providence, RI, 1997).
[18] L. Bolch, S. Greiner, H. de Meer, and K. Trivedi, *Queueing Networks and Markov Chains* (Wiley Interscience, Hoboken, NJ, 2006).
[19] U. N. Bhat, *An Introduction to Queueing Theory* (Wiley Interscience, Hoboken, NJ, 2008).
[20] R. Guimerà, A. Díaz-Guilera, F. Vega-Redondo, A. Cabrales, and A. Arenas, Phys. Rev. Lett. **89**, 248701 (2002).
[21] M.-B. Hu, W.-X. Wang, R. Jiang, Q.-S. Wu, and Y.-H. Wu, Phys. Rev. E **75**, 036102 (2007).
[22] L. Zhao, Y.-C. Lai, K. Park, and N. Ye, Phys. Rev. E **71**, 026125 (2005).
[23] H. Zhang, Z. Liu, M. Tang, and P. Hui, Phys. Lett. A **364**, 177 (2007).
[24] M. Takayasu, H. Takayasu, and K. Fukuda, Physica A **233**, 824 (1996).
[25] M. Takayasu, H. Takayasu, and K. Fukuda, Physica A **277**, 248 (2000).
[26] M. R. Evans and T. Hanney, J. Phys. A **38**, R195 (2005).
[27] Albert-László Barabási and R. Albert, Science **286**, 509 (1999).
[28] P. Erdős and A. Rényi, Publ. Math. Inst. Hung. Acad. Sci. **5**, 17 (1960).
[29] D. J. Watts and S. H. Strogatz, Nature (London) **393**, 440 (1998).
[30] L. Lovász, in *Combinatorics, Paul Erdős is Eighty*, Vol. 2 (Bolyai Society, Budapest, 1993).
[31] L. Lovász (private communication).